Journal of Materials Chemistry A

ROYAL SOCIETY OF CHEMISTRY

PAPER

View Article Online
View Journal

Cite this: DOI: 10.1039/d5ta07131c

Effect of binder viscosity on the rheology of cathode slurries and performance of lithium-ion battery half cells

Abarasi Hart, [ab] Xuesong Lu, [ab] Georgia Englezou,[a] Laura Wheatcroft, [ab] Chirag Patel,[ab] Joe C. Stallard,[bc] Samuel G. Booth, [ab] Charles Stothard,[ab] Norman A. Fleck, [bc] Stephen J. Ebbens, [a] Beverley J. Inkson, [ab] Serena A. Cussen, †[ab] Denis J. Cumming [ab] and Alisyn J. Nedoma *[ab]

Reliably benchmarking the performance of new cathode materials is an ongoing challenge in the development of high-capacity lithium-ion batteries. Small variations in the formulation or processing of a cathode can severely affect the performance of the resulting battery cell. Understanding and controlling interactions between the binder and other slurry components will enable faster, more rationalised battery cell optimisation. For the first time, this work systematically varies the viscosity of polyvinylidene fluoride (PVDF) binder solutions across a decade (15 to 320 mPa s) whilst holding constant the solid loading of carbon black (CB) and cathode active material ($LiNi_{0.8}Mn_{0.1}Co_{0.1}O_2$; NMC811). Steric stabilisation, rather than depletion or flocculation, is shown to be the mechanism by which PVDF modulates the structure of CB colloidal particles in a slurry. Gelled CB structures, evident in shear-thinning behaviour, are observed for all slurries, but two distinct CB gel regimes are evident: percolated and dispersed. The percolated regime occurs when the ratio of dissolved PVDF to free CB is reduced, *e.g.* by the incomplete dissolution of the PVDF. These samples exhibit thixotropic flow behaviour and lead to more porous cathodes. Well-dispersed CB gels exhibit reversible flow behaviour and form denser cathodes. The mass loading of cathodes increases with solution viscosity, and above a viscosity of 128 ± 46 mPa s, the mass loading across the cathode tape becomes uniform. The first discharge capacity of battery cells increases monotonically with the viscosity of the PVDF solution, but no correlation is evident after 100 cycles. Process models that incorporate these relationships will improve the reproducibility of cathode coatings, enable higher coating weights and reduce materials losses leading to lower manufacturing costs and higher capacity batteries.

Received 1st September 2025
Accepted 7th January 2026

DOI: 10.1039/d5ta07131c

rsc.li/materials-a

1 Introduction

The widespread adoption of electric vehicles is limited by consumers' range anxiety: the fear that vehicle batteries cannot store sufficient charge to transport the consumer between destinations.[1] Lithium-ion batteries lead competing battery chemistries in terms of energy density,[2] with the potential to deliver small, light-weight automotive batteries that will alleviate range anxiety. Cathode materials remain the focus of battery optimisation, as they are the capacity-limiting component and can account for >50% of the cell cost.[3] Emerging high-nickel chemistries combine high specific capacity with fine control of particle morphology;[4] however, the commercialisation of these materials is limited by a fundamental lack of knowledge about how to process them at scale.[5]

Rapid electrochemical screening of new cathode materials is essential for targeting synthetic efforts and informing data-driven materials design.[6] Standardised electrochemical testing protocols have removed some of the variability in reported values of performance metrics, like the first specific discharge capacity and percentage capacity fade, but it remains challenging to rapidly and accurately assess the performance of new cathode materials. The composition of the electrode and its processing conditions must be optimised for each new cathode material, and there is presently no overarching set of design rules to streamline this process.[7] Whilst each step in the formation of the electrode has the potential to introduce variability, the first step, slurry formulation, appears to be critical for controlling the structure of the electrode.[8,9]

[a]School of Chemical, Materials and Biological Engineering, University of Sheffield, Western Bank, Sheffield, S10 2TN, UK. E-mail: a.nedoma@sheffield.ac.uk; Tel: +44 (0)7810845678

[b]The Faraday Institution, Quad One, Harwell Science and Innovation Campus, Didcot, OX11 0GD, UK

[c]Department of Engineering, Cambridge Centre for Micromechanics, University of Cambridge, CB2 1PZ, Cambridge, UK

† Present address: School of Chemistry, University College Dublin, Science Centre-South Belfield, Dublin 4, Ireland.

The formulation and processing of the slurry affects the dispersion of the cathode active material and the conductive additive, impacting the electrochemical performance of the electrode.[9–12] From a processing perspective, the viscosity of the slurry must be high enough to suspend the cathode particles as the wet film dries (counteracting sedimentation)[8] but sufficiently low to flow smoothly through standard film-deposition equipment.[11,13,14] Viscosity is generally adjusted by changing the amount of solvent,[15] which changes the solids loading in the slurry. A high solids loading is preferable because it reduces energy consumption during film drying.[16] Tuning the viscosity of the slurry by controlling the binder rather than the solvent provides a route to maximise solids loading. Judicious binder selection could even reduce the total mass of binder used in a cathode tape, increasing its specific energy density.

Polyvinylidene fluoride (PVDF) is the most conventional binder used for LIB cathodes and it is dissolved in *N*-methyl pyrrolidone (NMP). Although NMP is a good solvent for PVDF, a gel fraction is often observed,[17] which has been attributed to kinetically trapped crystalline domains that act as crosslinks.[18] Incomplete dissolution of the binder reduces the viscosity of the slurry and may result in PVDF-rich inhomogeneities in the dry cathode.

A common benchmark material for high-nickel cathodes is $LiNi_{0.8}Mn_{0.1}Co_{0.1}O_2$ (NMC811), a layered oxide that belongs to the $R\bar{3}m$ space group. The reversible specific capacity of NMC811 is ~200 mA h g^{-1}. Relative to other NMC-family materials, the high nickel content of NMC811 increases its specific capacity but lowers its operational voltage window[19] and accelerates capacity fade.[20] In the charged state, the crystal lattice is stressed[21] and susceptible to cracking.[22] Cracks increase the surface area of material exposed to electrolyte, growing the cathode–electrolyte interfacial layer, ultimately degrading performance. Although single-crystal NMC811 exhibits greater capacity retention upon cycling, polycrystalline NMC811 has a higher discharge capacity, even at elevated *C*-rates.[23]

Carbon black (CB) is a cathode additive that increases the electrical conductivity of the composite cathode. Battery-grade CB comprises primary particles ~20 nm in diameter that are fused into fractal secondary particles with a hydrodynamic radius of 150 nm.[24] Hydrophobic and highly porous, carbon black exhibits a range of dispersion behaviours depending on its affinity for a solvent.[25,26] Reynolds *et al.* were able to disperse SuperC65 (a commercial CB product) in NMP[14] such that the dispersion was featureless under optical microscopy. In contrast, Sung *et al.* observed ~10 μm aggregates of SuperC65 in NMP.[27] This discrepancy demonstrates that the dispersion of CB in NMP is not a robust process and likely depends on parameters that are not fully controlled, such as the moisture content of the reagents.

PVDF moderates the interactions of CB with NMP in a cathode slurry. There is a weak affinity between CB and PVDF[27] that drives the polymer to adsorb onto the surface of the solid.[28] At very low concentrations of polymer, surface coverage is incomplete and drives flocculation of the colloid;[29] however, at polymer concentrations relevant to a cathode slurry, the adsorbed polymer sterically stabilises CB aggregates. The structure of CB aggregates varies depending on the composition and processing of the slurry, but in all cases the resulting slurry becomes a shear-thinning gel due to the presence of CB.[30] If the concentration of CB is above the critical volume fraction for percolation, the cathode gel is glassy, electronically conducting and behaves like a solid at rest.[31] Below the percolation threshold, agglomerates of CB act like crosslinkers in the polymer matrix and increase the elasticity of the cathode gel.[31] The conductivity of the slurry does not necessarily relate to the conductivity of the dry electrode. Chang *et al.* found that using a dispersant for CB reduced the viscosity of the slurry, decreased the charge-transfer impedance of the cell and improved capacity retention.[32]

Cathode slurries are generally not equilibrium colloidal systems, rather they are kinetically trapped by their processing route. The deagglomeration of CB powder and the resulting particle size distribution critically affects the structure of the slurry.[33,34] Dry mixing the CB and polycrystalline cathode powders partially deagglomerates the CB, which coats the cathode particles and increases the conductivity of the dry cathode tape.[35] The CB that adheres to the cathode particles no longer contributes to gelation, and the viscosity of the slurry decreases.[36,37] Further deagglomeration occurs during planetary mixing. Shear stress applied by the fluid medium on the CB particles cause them to fragment.[30,38] Increasing the viscosity of the binder solution can increase the shear stress applied to CB particles,[38] but slurries with higher viscosity also dissipate more mechanical energy as heat. Long mixing times and high shear rates have been used to reduce the viscosity of the slurry[39] by decreasing the mean particle size of CB.[40]

After mixing, the slurry is coated under application of shear stress. The gel structure of CB makes the quiescent slurry elastic and self-supporting. Applying sufficient shear stress causes the slurry to flow. If the CB structure percolates through the gel, it exhibits a yield stress. Above the yield stress, the CB network fragments into smaller, free flowing aggregates. The reverse process of re-forming structure is kinetically limited, so the slurry exhibits thixotropy, *i.e.* irreversibility of the viscosity flow curves.[26,31,41] In contrast, if the CB agglomerates are dispersed in the polymer solution, they remain dispersed and the viscosity flow curves are reversible.[31] Based on both battery performance and ease of processing, a fully dispersed CB gel is likely to outperform a percolated gel. Controlling the viscosity of the slurry using the binder rather than the gelation of CB enables the use of slurries with smaller, more dispersed CB nanoparticles.

We systematically vary the viscosity of the PVDF solution from 15–320 mPa s for cathodes comprising mass ratios of 95 : 5 : 5 NMC811 : CB : PVDF and measure the effect on the rheological behaviour of the slurries and the structure of the resulting electrode films and battery half cells. The results underscore the importance of binder selection and suggest a route for rapidly optimising the formulation of new cathode chemistries.

2 Experimental

2.1 Materials

Polycrystalline $LiNi_{0.8}Mn_{0.1}Co_{0.1}O_2$ (NMC; PI-Kem, USA) was used as the cathode active material and Timcal Super C65 (CB;

Table 1 Physical properties of NMC and CB powders used

Particle species	Tap density kg m^{-3}	Diameter	Specific surface area m^2 g^{-1}
NMC	2310[a]	13 μm[b]	0.49[a]
CB	1600[a]	150 nm[c]	62[a]

[a] Properties reported by the manufacturer. [b] Volume-averaged diameter (see SI Fig. 1 for measured distribution). [c] Secondary particle diameter reported by Spahr *et al.*;[24] primary particles are 37 nm in diameter.

Imerys, France) was the carbon black conductive additive. The physical properties of the powders are reported in Table 1. A range of polyvinylidene fluoride (PVDF) homopolymers was purchased from Sigma-Aldrich, USA (H15, H20, H70, H80); MTI Corporation, USA (H180) and Solvay, France (H320, Solef 5130). The solvent was anhydrous *N*-methyl-2-pyrrolidone (NMP; Sigma-Aldrich, 99.5%). Double-side conductive carbon-coated aluminium foil (MTI Corporation) was used as the current collector. The electrolyte was $LiPF_6$ in ethylene carbonate : ethyl methyl carbonate (1 : 1 v/v) with 2% vinyl carbonate (Solvionic, France). Lithium metal discs (15.6 mm in diameter, 250 μm thick, MTI Corporation) were used as the anodes for battery half cells. Glass fibre filter paper (GF/F, Whatman, UK) was cut into 16 mm discs and used as the separator for battery half cells.

2.2 Slurry preparation

A stock solution of 3.9 wt% PVDF in NMP was weighed out for each molecular weight of PVDF and mixed for 48 h on a magnetic stir plate. Samples are named as Hxx, where 'H' denotes a homopolymer and xx gives the solution viscosity in mPa s. The PVDF/NMP solutions are characterised in Table 2. Several of the solutions did not completely dissolve, evidenced by haziness and the inability to pass through a 0.45 μm hydrophilic syringe filter. The viscosity of homopolymer solutions was measured using both rotational viscometry and capillary viscometry (see SI Section 5.) Solutions used to make battery cells were prepared inside an argon-filled glovebox (O_2 and H_2O < 0.1 ppm).

Solutions were also prepared from blends of the highest (H320) and lowest (H15) molecular weight homopolymers in order to access additional viscosities within the range. Blends were prepared by weighing appropiate amounts of each homopolymer solution (3.9 wt%) into a single vial and stirring. The resulting blend also comprised 3.9 wt% PVDF, but the viscosity could be smoothly controlled between 15 and 316 mPa s depending on the relative amounts of each homopolymer (see SI Fig. 3 for the viscosity–composition calibration.) The composition and viscosity of blends are given in Table 3. Blends are named as Bxx where 'B' denotes blend and xx is the viscosity of the solution in mPa s.

For each series of cathode slurries, a stock powder mixture of NMC and CB (18 : 1 w/w) was prepared to ensure uniform starting properties for each sample. The NMC and CB were weighed into an agate mortar and pestle and mixed by hand for 15 min to co-disperse the solids. For each slurry, 143 mg of mixed NMC/CB powder was transferred into a 12 mL polypropylene container (Thinky, Japan), 175 μL of the selected PVDF stock solution was pipetted into the powder mixture and the sample was weighed to confirm the final mass fraction of each component. The dried cathode had a 95 : 5 : 5 weight ratio of NMC : CB : PVDF. The sealed slurry was blended using a Thinky ARE-250 planetary mixer at 2000 rpm for 6 minutes followed by a degassing step for 30 seconds at 2200 rpm. Dispersions omitting either NMC or CB were also prepared to study the individual contributions of components. The mass composition of each type of dispersion is listed in SI Table 5.

2.3 Film coating

A tape casting coater with a doctor blade (MTI Corporation) was used to coat the slurry onto the current collector under ambient conditions. The adjustable film applicator was placed on the current collector and set to a gap height ranging from 200–285 μm. The slurry was collected with a metal spatula and scooped onto the current collector in front of the doctor blade and coated at a speed of 5.8 mm s^{-1}. The wet film was dried for 2 h under air heated to 80 °C and advected over the film. The solid film was transferred to a vacuum oven at 80 °C for at least an additional 24 h. Cathode discs (12 mm diameter) were cut using an MTI Corporation coin cell punching machine. Each cathode was weighed and its thickness was measured using a micrometer. Cathodes were returned to the vacuum oven for at least 12 h to remove ambient humidity prior to transferring them into the glovebox.

Table 2 Properties of PVDF homopolymers and their solutions

Sample name	Appearance	Filtered	$\bar{M}_w$ kg mol^{-1}	R_h nm	η^a mPa s
H15	Clear	Yes	180[b]	9.5	14.5
H20	Transparent yellow	Yes	275[b]	12.0[c]	22.0
H70	Mildly hazy	No	530	17.1[c]	70.6
H80	Mildly hazy	No	534	17.2[c]	81.4
H180	Hazy	No	600	18.3[c]	175
H320	Clear	Yes	1300	27.9	316

[a] All solutions comprise 3.9 wt% PVDF in NMP. [b] Sigma-Aldrich provided the polydispersity index for these polymers: $Đ = 2.54$ (H15) and $Đ = 2.57$ (H20). [c] Values were interpolated based on parameters obtained from dynamic light scattering because these resins contained a gel fraction evidenced by haziness; see SI Section 2 for calculations.

Table 3 Composition and viscosity of blended PVDF solutions in NMP

Blend name	x_{H320} [a]	x_{H15}	η [b] mPa s
B20	0.015	0.985	22.0
B40	0.236	0.764	39.8
B70	0.469	0.531	74.1
B130	0.673	0.327	129
B180	0.780	0.220	178

[a] The mass fractions of homopolymer solutions H320 and H15 are given by x_{H320} and x_{H15}, respectively. [b] All solutions comprise 3.9 wt% PVDF in NMP.

2.4 Half-cell assembly

Battery half cells were prepared using CR2032 hardware (Cambridge Energy Solutions, UK) inside an argon glovebox (H_2O and O_2 < 1 ppm). The lithium metal anode was buffed flat using a toothbrush to remove oxidation and placed onto a spacer in the cell. The separator was placed atop the lithium and 100 μL of electrolyte were pipetted onto the separator. The cathode disc was placed (cathode down) onto the separator, the coin cell was closed, manually flipped over and sealed in a coin-cell crimper (MTI Corp.)

2.5 Characterisation

2.5.1 Rheology. A Modular Compact Rheometer MCR 502 (Anton Paar, Austria) was used to carry out rheological measurements using the cone and plate measurement system CP12-6 with a cone-angle of 4°, gap of 215 μm, plate diameter of 12.1 mm and a temperature of 25 °C. Viscoelastic measurements were carried out first, as these were constrained to conditions that did not damage the sample. A frequency sweep was carried out between 100 and 0.1 s^{-1} at a constant strain rate of 1%, within the linear viscoelastic region. Next, flow curves were measured by pre-shearing the sample at a strain rate of 5 s^{-1} for 30 s then ramping the strain rate from 1 to 500 s^{-1} in 2.5 s intervals. The sample was continuously sheared at 500 s^{-1} for 180 s then ramped from 500 to 1 s^{-1} in 2.5 s intervals.

A range of Canon-Fenske glass capillary viscometers was used to measure the drop times for solutions of 3.9 wt% PVDF in NMP. Approximately 12 mL of solution were transferred to the viscometer, which was submerged up to the top of the upper reservoir in a 25 °C isothermal water bath. Samples were thermally equilibrated for 10 min and then the drop time was measured three times and averaged. The calibration factor for each viscometer was measured using a glycerol or glycerol/water blend, and used to convert the drop time into kinematic viscosity. The measured kinematic viscosities were converted to dynamic viscosities by multiplying by the density of the solution, assumed to be a linear interpolation of the component densities. Values of viscosity measured using this technique agreed well with values measured using rotational viscometry (see SI Fig. 4.)

2.5.2 Galvanostatic cycling. Battery half cells were transferred from the glovebox to a potentiostat (Maccor Series 4000 test system, USA) with terminals inside an ambient temperature chamber (Binder 2000, Germany) at 25 °C. Cells were rested for 8 h to allow the electrolyte to permeate the cathode. Two complete formation cycles were carried out by charging the cells to 4.3 V (*vs.* Li/Li^+) and discharging to 3 V at C/20, then 100 cyles were carried out at 1C within the same voltage window.

2.5.3 Particle size analysis. A Mastersizer 3000 (Malvern Panalytical, UK) laser-diffraction particle size analyser was used to measure the NMC particle size distribution (see SI Fig. 1 for the measured distribution). A ZetaPALS laser diffraction instrument ($\lambda = 660$ nm, Brookhaven Instruments Corporation, USA) was used to measure the hydrodynamic radius of dilute PVDF coils in NMP. To measure the hydrodynamic radius of carbon black agglomerates formed during mixing, small amounts of freshly prepared slurry were diluted to ~0.05 wt% in NMP, thoroughly shaken, and left for a day to allow the larger cathode particles to settle. The transparent supernatant was decanted into a polystyrene cuvette for measurement. The raw autocorrelation data were fitted to a cumulative distribution function using the inbuilt machine software. The average hydrodynamic radius and distribution breadth were recorded.

The microstructure of dry cathodes was imaged using an FEI Inspect F50 scanning electron microscope (SEM) equipped with secondary electron (SE) and backscattering (BSE) image detectors. A 6 nm carbon coating was deposited onto samples.

2.5.4 Adsorption measurements. The adsorption of PVDF onto solids in the slurry was quantified by separating the solids from the liquid and measuring the concentration of polymer remaining in the liquid phase. The slurry was centrifuged (Sigma 1-14 Microfuge, Germany) for three hours at 14 800 rpm and the clear supernatant was decanted. The concentration of PVDF in the supernatant was determined by measuring the viscosity of the supernatant at a frequency of 100 s^{-1} and interpolating the polymer concentration from viscosity–concentration calibrations that were measured for each molecular weight of PVDF.

A control experiment was carried out to verify that centrifugation conditions did not cause the polymer coils to precipitate from solution (see SI Fig. 6 for viscosity measurements before and after centrifugation).

3 Results and discussion

3.1 Slurry rheology

Rheological properties of the cathode slurries, like viscosity and viscoelasticity, are not only necessary for controlling film deposition but also provide insight into the microstructure of the optically opaque slurries. Fig. 1 shows the viscosity flow curves for cathode slurries in which the viscosity of the initial PVDF/NMP solution, η_{PVDF}, is varied and the solid loading is held constant at 43 wt%. In Fig. 1a, the viscosity is varied by changing the molecular weight of the homopolymer binder and in Fig. 1b, the viscosity is controlled by blending two homopolymers in different ratios.

All of the slurries exhibit shear-thinning behaviour that can be uniquely attributed to the presence of a CB gel. Several of the homopolymer slurries exhibit a subtle shoulder, suggesting the breakup of a weakly aggregated CB structure,[14,27,31,42] as shown

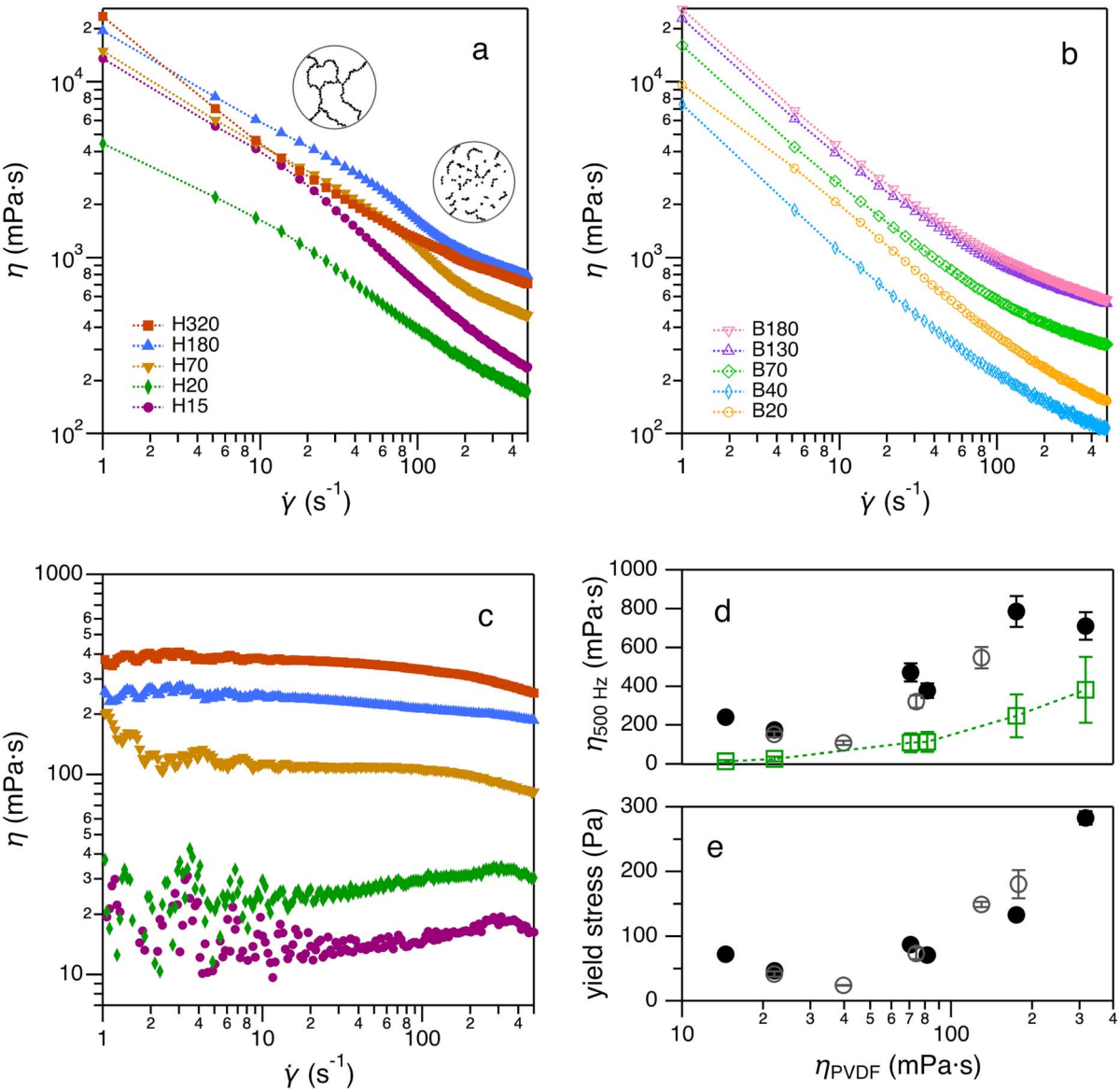

Fig. 1 Rotational viscometry data for cathode slurries comprising NMC811/CB/PVDF in the weight ratio 95 : 5 : 5 and 43 wt% solid loading in a solution of 3.9 wt% PVDF in NMP. (a) Viscosity flow curves for slurries comprising homopolymer PVDF labelled as Hxx and (b) blends of PVDF labelled as Bxx, where xx is the viscosity of the initial binder solution in mPa s. The inset of (a) schematically depicts the structure of CB. (c) Viscosity flow curves for NMC811 dispersions comprising the homopolymer binders given in (a). (d) Slurry viscosity at a strain rate of 500 s^{-1} for slurries made from homopolymers (●) and blends (○). Fitted values of the viscosity of the analogous NMC dispersions are included for reference with lines as a guide for the eye (□). (e) Yield stress *vs.* the viscosity of the binder solution for slurries made from homopolymers (●) and blends (○).

in the inset of Fig. 1a. The presence of the shoulder does not correlate with η_{PVDF}, but may be related to the fraction of semicrystalline PVDF, which varies for the different homopolymers. In contrast, all of the blended slurries exhibit a smooth, featureless decrease indicative of well-dispersed CB agglomerates. The blends were made from two fully soluble homopolymers. Slight differences in the fraction of available polymer may explain the aggregation of CB in some slurries.

A set of homopolymer slurries analogous to the ones in Fig. 1a is shown in Fig. 1c, except that no CB was added (*i.e.* the dispersions comprise only NMC, PVDF and NMP.) These NMC dispersions exhibit Newtonian behaviour (viscosity is constant with strain rate) across the same range of frequencies, indicating that the shear-thinning behaviour of the slurries is uniquely due to the gelation of CB rather than entangled polymer chains, as the latter are present in both cases. The NMC dispersions are an order of magnitude less viscous than the slurries, but one to two-fold more viscous than the unfilled binder solutions (see SI Sect. 11 for the effect of NMC on the viscosity of polymer solutions). The presence of micron-scale NMC particles increases the viscosity of the dispersions by dissipating momentum through drag (Stoke's flow), but the effect is relatively limited because the particles remain free flowing. The order-of-magnitude increase in viscosity caused by adding CB to the slurries is the result of a gelled CB structure that resists flow and mechanical deformation.

The viscosity of the NMC-only dispersions (Fig. 1c) increases monotonically with η_{PVDF}, indicating that PVDF controls the viscosity of the dispersions. Notably, the viscosity of the cathode slurries does not change monotonically with the viscosity of the PVDF solutions because the gel structure of CB is not wholly determined by the viscosity of the binder solution. Single point viscosity values are plotted for each slurry at the highest strain rate studied (500 s^{-1}) in Fig. 1d. At this strain rate, the CB structure that gave rise to a shoulder in the flow curve is expected to have yielded. The steady-state viscosity at higher rates of strain has been related to the reversible assembly and fragmentation of CB aggregates.[26] The addition of CB only contributes 1.9 vol% to the slurry, which would have less than a 1% effect on the viscosity of the slurry if the CB were free flowing (calculated using the Krieger–Dougherty equation, see SI eqn (3)). In fact, the viscosity of most of the slurries at a strain rate of 500 s^{-1} is several factors greater than the viscosity of the analogous NMC dispersions, indicating that even at high strain rates, CB retains a gelled structure.

The yield stress is a construct that depends on variables like the ramp rate and the history of the fluid, but it can be useful for drawing comparisons between slurries.[43] The yield stress for each slurry is plotted against the viscosity of the PVDF solution in Fig. 1e (see SI Section 9 for details of the fitting). There is a subtle, but significant minimum in yield stress that is reflected in the shape of the single-point viscosity data (Fig. 1d). The viscosity of the binder solution tends to increase the viscosity of the slurry monotonically, so we can infer that the CB structures have a decreasing contribution to viscosity, resulting in the observed minimum. Whilst this trend is useful for studying slurry structure, we note that it is not a fundamental property of the system, but rather a snapshot of kinetically trapped materials.

Hysteresis between the flow curves during the upward and downward ramps of strain rate is a signature of a percolated CB structure.[31] The stress–strain curves are shown for two slurries with the same viscosity (180 mPa s), but the slurry in Fig. 2a is formed from a homopolymer binder (H180) whilst that in Fig. 2b comprises a binder blend (B180). H180 exhibits significant hysteresis whereas the forward and reverse ramps for B180 overlap. The insets depict the CB structures that are likely responsible for this behaviour. H180 forms a percolated CB structure that fragments into smaller agglomerates under shear. B180 comprises disperse CB agglomerates that do not change dimensions when sheared.

None of the blended binder slurries exhibit flow hysteresis within uncertainty (see Fig. 2c), whilst three of the homopolymer slurries exhibit significant thixotropy (these slurries also have prominent shoulders in their viscosity flow curves). This finding demonstrates that CB structure formation is affected not only by the viscosity of the binder solution but also by the unique properties of the binder feedstock (*e.g.* crystallinity or chain branching). Legrand *et al.* have shown that the transition from percolation gelation (thixotropic samples) to well-dispersed CB gels is sensitive to the CB : PVDF ratio.[31] Given that these cathode slurries are prepared with a 1 : 1 ratio of CB : PVDF, small changes in the solubility of the PVDF are likely to affect the structure of the CB gel. Blending binders of different molecular weights appears to be a simple way to reliably control the flow properties of cathode slurries.

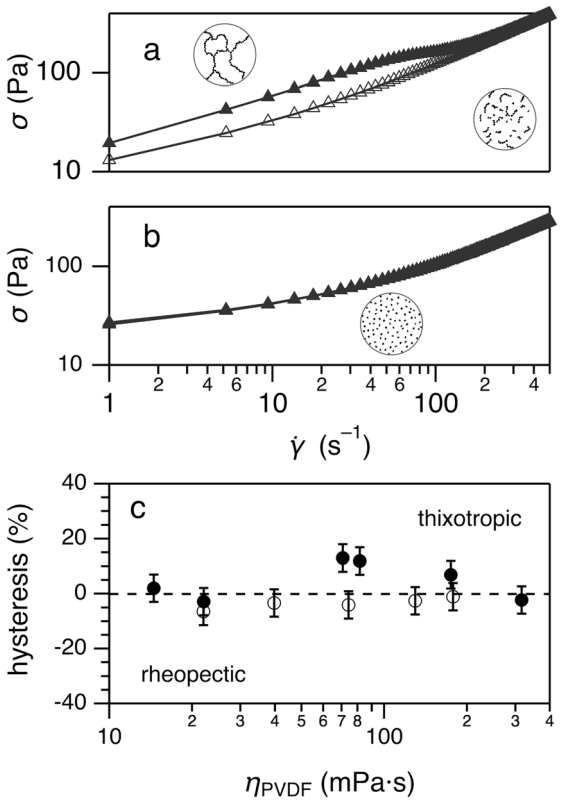

Fig. 2 Stress–strain flow curves for cathode slurries comprising (a) homopolymer H180 and (b) blend B180 during upward (▲) and downward (△) ramps in the strain rate. Lines are a guide for the eye. Insets depict proposed structure of CB agglomerates. (c) Hysteresis as a percent difference in the areas of the upward and downward ramp stress–strain curves for slurries comprising homopolymer (●) and binder blends (○). The dotted line indicates zero hysteresis.

Viscoelastic measurements (small amplitude oscillatory shear) offer a complementary rheological quantity that reflects the quiescent behaviour of slurries without inducing flow. The binder solutions (SI Fig. 4) and NMC dispersions (Fig. 1c) exhibit Newtonian flow with the application of shear, but the elasticity of the CB network enables slurries to resist permanent deformation when small strains (<1%) are applied. The ratio of the loss and storage moduli, tan δ, across angular frequencies, ω, is plotted for homopolymer slurries in Fig. 3a and blended binder slurries in Fig. 3b.

The slurries all exhibit elastic behaviour (tan $\delta < 1$) due to the gelation of CB. As expected, there is no evidence of the structural breakdown that gave rise to hysteresis in some of the flow curves because viscoelastic measurements do not induce flow. The extrapolation of tan δ to zero frequency provides a rough parameterisation of the viscoelasticity of the quiescent slurries. Fig. 3c plots $(\tan\delta)_0$ *vs.* η_{PVDF}. Values initially decrease and then flatten around a threshold viscosity of (55 ± 15 mPa s), above which the slurry exhibits relatively constant viscoelastic behaviour. This threshold value for η_{PVDF} also corresponds to where

the yield stress changes slope (Fig. 1e), suggesting a common origin. Binder chain entanglements do not appear to affect $(\tan \delta)_0$ above the threshold viscosity, so it is more likely that a structural difference in the CB network causes the observed increase in elasticity.

We can disambiguate the contributions of each component in a slurry by comparing the viscosities of the PVDF solution, the NMC-only dispersion and the full cathode slurry. The viscosity of each cathode slurry (at a strain rate of 500 s^{-1}) can be approximated as a linear combination of contributions such that $1 = f_{\eta,\mathrm{PVDF}} + f_{\eta,\mathrm{NMC}} + f_{\eta,\mathrm{CB}}$, where $f_{\eta,x}$ is the fractional contribution to the viscosity of the slurry from component x (see Fig. 4). This strain rate reflects the highest shear stress applied to a slurry, for which the CB network is largely broken up and particles are free-flowing. The slurry viscosities at this strain rate provide a rough depiction of the size of CB particles: a small population of large particles dissipates less energy than a large population of small particles, so the most deagglomerated samples have the highest viscosity contribution from CB. For all slurries, the contribution from CB is greatest followed by the contribution from PVDF, and the contribution from NMC is small or negligible. The viscosity contribution of CB steadily drops across the series, which is broadly consistent with the expectation that the deagglomeration of CB is less efficient as the viscosity of PVDF increases.

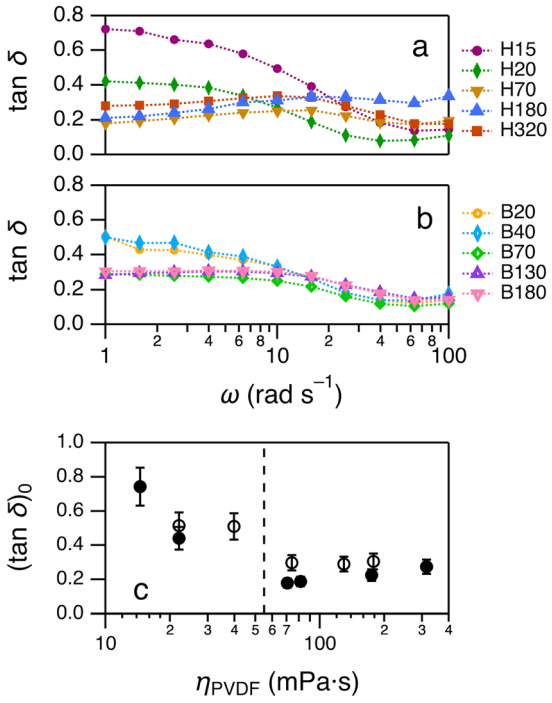

Fig. 3 Viscoelastic characterisation of cathode slurries comprising NMC811/CB/PVDF in the ratio 95 : 5 : 5 by weight and 43 wt% solid loading in solutions of 3.9 wt% PVDF in NMP with varying viscosities. (a) Loss tangent frequency sweeps for slurries comprising homopolymer binders Hxx and (b) blended binders, where xx denotes the binder solution viscosity in mPa s. Dotted lines are a guide for the eye. (c) Zero-frequency extrapolations of the loss tangent for slurries comprising homopolymers (●) and binder blends (○). The dotted line approximates the threshold viscosity above which tan δ does not vary.

These results show that the viscosity contribution of PVDF increases monotonically across the series of slurries whilst the contribution from CB decreases monotonically. The competition between these two trends gives rise to the observed minimum in both slurry viscosity (shown in Fig. 1e) and yield stress (Fig. 1d). These results highlight the importance of both formulation and processing (especially mixing) on the rheological properties of a cathode slurry.

3.2 Interactions between the binder and solid particles

Interactions between polymers and colloidal particles are known to drive aggregation behaviours, such as flocculation. Previously, Sung *et al.*[27] predicted only moderate adsorption of PVDF onto CB based on enthalpic interactions. The work of adhesion required to separate PVDF from CB is 78 mN m^{-1}, which is less than the work of adhesion to separate NMP from CB (86 mN m^{-1}). Consequently, it is enthalpically favourable for NMP to adsorb onto CB rather than PVDF. We revisit this argument in light of the high molecular weights of PVDF chosen for this study, which are entropically driven to adsorb onto CB in order to liberate a small molecule of NMP (the hydrophobic effect). Adsorption measurements are traditionally carried out at very low concentrations of polymer, but these conditions do not accurately reflect the structure of CB in a cathode slurry. Fig. 5 shows the gravimetric adsorption of homopolymer PVDF onto CB, NMC and a blend of CB/NMC when each dispersion is prepared in the same way as a cathode slurry (see SI Table 5 for the composition of each dispersion.) A control experiment in SI Sect. 7 verifies that centrifugation does not remove binder from solution.

The molecular weight of PVDF increases across the range of viscosities in Fig. 5. PVDF adsorbs to both CB and NMC, but the gravimetric adsorption is greater for CB because it has a much higher surface area than NMC (62 and 0.49 m^2 g^{-1}, respectively.[24,44]) Gravimetric adsorption onto either solid is expected

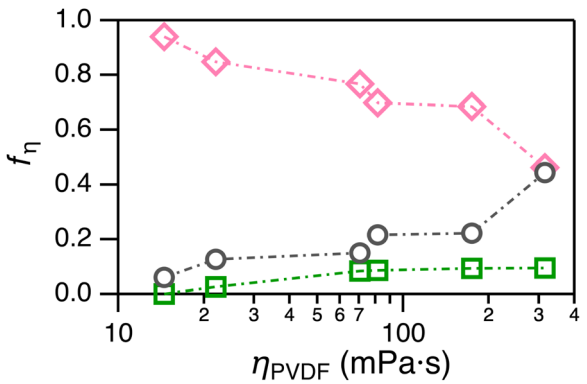

Fig. 4 Fractional contributions to the viscosity of cathode slurries at a shear rate of 500 s^{-1} for PVDF (○), NMC (□) and CB (◇). All polymer solutions comprise 3.9 wt% PVDF in NMP. Cathode slurries comprise NMC/CB/PVDF (90 : 5 : 5 by weight) with a solids loading of 43 wt%. The contribution from CB was inferred from the difference in viscosity between the slurry and the NMC dispersion, the NMC contribution was inferred from the difference between the NMC-dispersion and the PVDF solution.

to increase with the molecular weight of PVDF,[28,29] but we observe the opposite trend for both CB and NMC. We show that high viscosity limits the dispersion of powders (see Sect. 3.3). It seems likely that the monotonic reduction in adsorption is due to incomplete deagglomeration of the solids, which decreases the surface area available for adsorption.

Notably, the adsorption of PVDF onto solids in the cathode slurry is much less than its adsorption onto CB in the absence of NMC. As observed previously,[30] the dry mixing process coats a significant fraction of CB onto the surface of NMC, making the CB surface unavailable to interact with PVDF. This effective reduction in the amount of available CB reduces the viscosity of the slurry by as much as two decades (see SI Sect. 5 for viscosity flow curves comparing slurries to CB dispersions). It is worth noting that these gravimetric adsorptions correspond to very high areal adsorptions (4–40 $m^2\ g^{-1}$; see SI Fig. 14 for the areal adsorption of PVDF onto each solid) that are greater than a single monolayer. If these binder coatings persist through the drying process, it suggests that the molecular weight of the binder could be used to systematically control the thickness of binder on particles. This level of control would allow more decisive correlations to be drawn between the surface environment of cathode particles and the performance of battery cells.

A depletion-driven mechanism of flocculation has previously been reported for CB in PVDF/NMP;[45] however, in light of our results, depletion-driven flocculation does not seem possible, as the mechanism requires a non-adsorbing polymer. Nor is bridging flocculation credible due to the very high concentrations of polymer used in slurries. Consequently, we find that CB agglomerates are sterically stabilised by adsorbed PVDF.

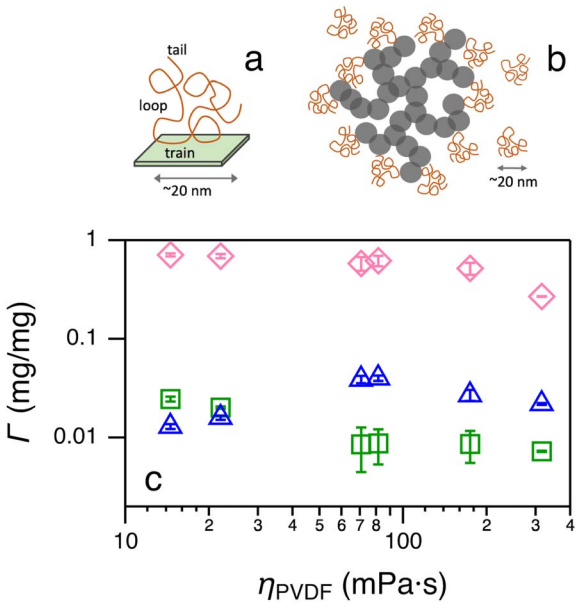

Fig. 5 Adsorption of PVDF binder onto solids. (a) Schematic of polymer adsorption onto a surface. (b) Schematic of sterically stabilised CB secondary particle. (c) Gravimetric adsorption of PVDF onto CB (◇), NMC (□) and blends of CB and NMC (△) as a function of the viscosity of the binder solution.

3.3 Deagglomeration of carbon black

The CB structure is difficult to quantify because it is optically opaque, but a snapshot of the particle size distribution can be obtained by diluting each slurry in NMP immediately after mixing. The diluted samples are aged for 24 h, which is long enough to allow cathode particles to settle and dilute enough to slow the kinetics of aggregation (see ageing controls in SI Section 14). The size distribution of CB is affected by both the mechanical mixing process and the viscosity of the solution. To disambiguate these effects, a series of three dispersions are prepared without any binder, so that the initial viscosity is that of pure NMP (1.89 mPa s). One sample is sonicated for 90 min and another undergoes the planetary mixing process used to mix slurries (see Fig. 6a). Sonication reduces the hydrodynamic radius of CB by 50% relative to planetary mixing due to the higher overall mechanical energy imparted to the dispersion. The smallest CB particle size (202 ± 71 nm) is obtained when NMC and CB are co-mixed with NMP in the planetary mixer. The resulting hydrodynamic radius is similar to that reported using transmission electron micrography (150 nm),[24] suggesting that the process is capable of fully deagglomerating the CB powder into secondary particles.

The addition of binder to slurries decreases the deagglomeration of CB. Fig. 6b shows that the radius of CB particles is larger than 202 nm for all of the slurries formulated with binder. Higher viscosity media exert a higher shear stress on the CB than low viscosity media when the same mixing conditions are used, which can lead to a greater degree of deagglomeration;[38] however, our results seem to be consistent with those of Grieβl *et al.*,[40] who observed a decrease in the average CB particle diameter with longer mixing times and higher mixing velocities. The mechanical energy required to deagglomerate CB increases with viscosity because more energy is dissipated as heat. This trend seems to plateau around 40 mPa s for the blended slurries; perhaps because the effects of viscous dissipation are balanced by the greater shear stresses. For comparison, the size of CB agglomerates in dispersions of CB/PVDF/NMP (without NMC) are also shown. These agglomerates are generally larger in diameter than those present in cathode slurries, even though the same mass of CB and PVDF were used in both cases and processing was identical. In the slurries, a fraction of the CB adsorbs onto the NMC, removing it from the dispersion. This effective decrease in the ratio of CB : PVDF appears sufficient to transition the gel from the regime of percolated CB agglomerates to dispersed agglomerates. The viscosity of the binder solution definitely affects the deagglomeration of CB, but other significant factors are present.

The plateau in CB particle sizes roughly coincides with the plateau in $(\tan\delta)_0$. In particular, the homopolymer slurries exhibit a slightly higher CB particle size and a slightly lower $(\tan\delta)_0$ than the blends. Fig. 6c explores the inverse relationship between the elasticity of slurries and the size of CB particles. A moderate correlation ($R^2 = 0.60$) exists, indicating that particle size is the leading order effect influencing the viscoelasticity of slurries. This finding is inconsistent with the expectation that the elasticity of colloidal gels scales inversely with the size of

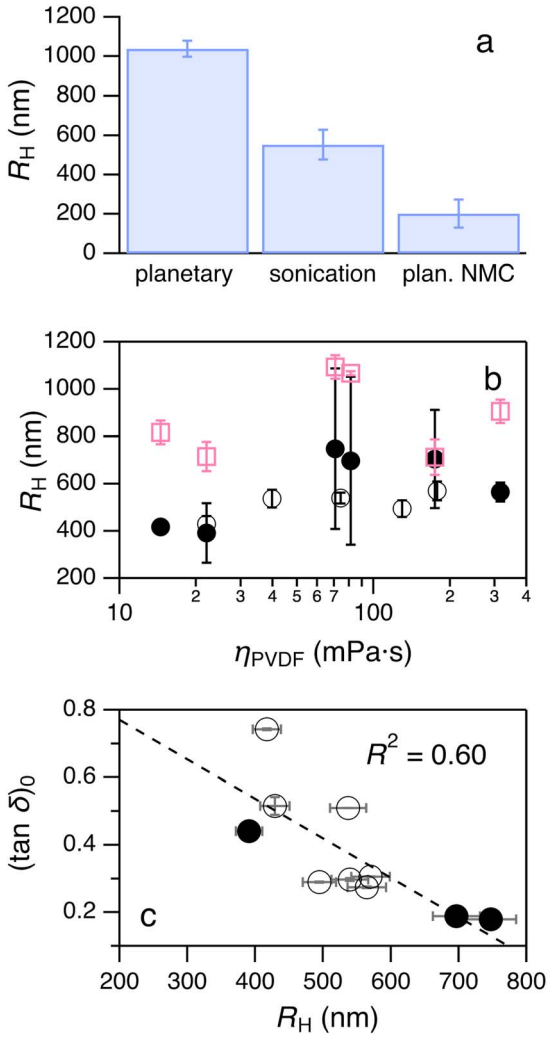

Fig. 6 DLS measurements of the hydrodynamic radius of carbon black particles. (a) CB is dispersed in pure NMP using different mixing conditions: planetary mixing, sonication, and dry mixing with NMC followed by planetary mixing. (b) CB was recovered from cathode slurries comprising NMC/CB/PVDF (90 : 5 : 5 by weight) with a solid loading of 43 wt%. The binder solution comprises either homopolymer PVDF (●) or a blend (○). The particle sizes of analogous dispersions of CB in PVDF/NMP solutions (without NMC) are shown for comparison (□). Error bars denote the half-width of the particle size distribution. (c) Correlation between the viscoelasticity of slurries and the size of carbon black particles. The solid line shows a linear regression with R^2 = 0.60.

agglomerates,[46] but in our case, the size of clusters is controlled by mechanical deagglomeration rather than thermodynamically driven kinetics, so structure evolution occurs in reverse (large powder agglomerates break down into nanoparticles). The CB gels observed in this work are intermediate between the aggregated powder feedstock and fully deagglomerated nanoparticles.

3.4 Cathode films and half-cells

The structure and rheological properties of cathode slurries are known to affect the morphology of the dried electrode.[9] The strain rate applied to slurries during coating is less than 6 s^{-1}, which is too low to irreversibly disrupt the CB structure, (see SI Fig. 9 for a heat map depiction of strain rates at varying experimental conditions. Scanning electron micrographs are shown in Fig. 7 for cathodes made from each PVDF homopolymer. For some of the cathodes, the film thickness varies significantly across the tape, so samples of each cathode were selected to keep the thickness constant at 87 ± 3 μm (see SI Table 6 for individual sample thicknesses). Secondary electron measurements are more sensitive to the topography of the surface, including the carbon–binder domain (CBD), whilst backscattering measurements are more sensitive to the presence of electron-rich NMC.

Cracks form in samples when $\eta_{PVDF} \leq 22$ mPa s; low–molecular weight, semicrystalline polymer films are more likely to crack than high–molecular weight analogues because shorter polymer chains can crystallise more completely, embrittling the film.[47] The CBD in these samples largely segregates to the top air interface, attributed to advection due to solvent evaporation,[14] whilst NMC sediments under gravity to the lower interface with the current collector. The settling velocity of particles depends inversely on the viscosity of the medium in a simple, two-phase dispersion (see SI Sect. 17 for settling rate calculations for each cathode.) In the case of cathode slurries, both polymer chain entanglements and the CB structure can resist the sedimentation of NMC. The viscosity of the PVDF solution alone accounts for more than a twenty-fold difference between the settling velocities in the least (H15) and most (H320) viscous solutions.

The two cathodes formed from solutions on the range η_{PVDF} = 70–80 mPa s appear fluffy with CBD coating the NMC particles. These are the most porous samples (see Fig. 8b). The NMC particles in the backscattered images are relatively small because the larger particles settle to the bottom interface (see SI Fig. 16 for SEM images of the cathode interface that was peeled off the current collector.) The two cathodes formed from solutions for which $\eta_{PVDF} \geq 175$ mPa s exhibit a relatively homogeneous distribution of NMC particles and no apparent segregation from the CBD. Topographically, cathodes increase in homogeneity as the viscosity of the PVDF/NMP solution increases.

The average areal mass loading, m_{areal} varies with η_{PVDF}, as shown in Fig. 8a. There is significant variability in the mass loading across the cathode tape when $\eta_{PVDF} \leq 81$ mPa s and greater reproducibility when $\eta_{PVDF} \geq 175$ mPa s. For example, the standard deviation in mass loading is 68.9 g m^{-2} (1.38 mA h cm^{-2}) for cathodes made from H15, and 9.50 g m^{-2} (0.190 mA h cm^{-2}) for those made with H320. Not only is the mass loading higher for more viscous PVDF solutions, but the cathode tape is more uniform, enabling better control of the product quality during commercial production.

Given that all of the cathode slurries with $\eta_{PVDF} \geq 70$ mPa s exhibit similar viscoelastic properties (see Fig. 3c), the higher viscosity of the samples with $\eta_{PVDF} \geq 175$ mPa s uniquely enables a higher, more consistent mass loading. Anecdotally, lower viscosity films are observed to spread laterally on the current collector during drying, whereas higher viscosity films retain their original footprint. The cohesive energy density of

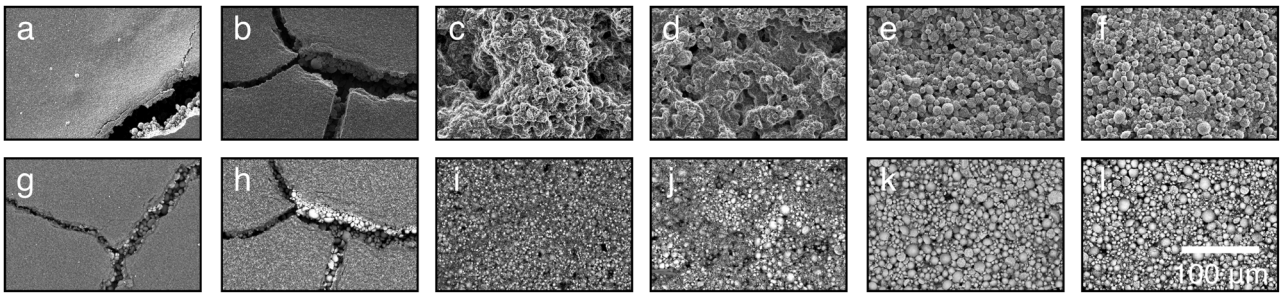

Fig. 7 Scanning electron micrographs for NMC/CB/PVDF (90/5/5 wt%) films. Sample names are Hxx where xx is the viscosity of the PVDF/NMP solution in mPa s. Secondary electron (SE) and backscattering (BSE) micrographs, respectively are shown for samples: H15 (180 kg mol^{-1}) (a) and (g); H20 (275 kg mol^{-1}) (b) and (h); H70 (530 kg mol^{-1}) (c) and (i); H80 (534 kg mol^{-1}) (d) and (j); H180 (600 kg mol^{-1}) (e) and (k); and H320 (1300 kg mol^{-1}) (f) and (l). The scale bar shown in (l) indicates 100 μm and applies to all images.

a slurry increases with viscosity, reducing lateral flow. Above $\eta_{PVDF} = 128 \pm 47$ mPa s, lateral flow has an insignificant effect on mass loading.

The porosity of cathodes is studied independently from their mass loadings by identifying a set of punched cathodes with the same mass loading, $m_{areal} = 135 \pm 2$ g m^{-2}. Despite having roughly the same mass of material, the thickness of the dry cathodes, Δt, varies non-monotonically with η_{PVDF} (see Fig. 8b). A well-tapped layer of NMC powder (tap density 2310 kg m^{-3}, according to the manufacturer[44]) would be 52 μm thick; the real cathodes range in thickness from 72 to 126 μm, indicating significant vertical expansion of the CBD. Thicker films correspond to higher porosity.

The two most porous cathodes are made from the two slurries in the series with statistically thixotropic behaviour, attributed to a percolated CB structure (see Fig. 2c). The samples with the highest (H180 and H320) and lowest viscosities (H15 and H20) comprise dispersed CB agglomerates and form denser cathode films. The type of CB structure appears to be the leading determinant of film thickness, with more dispersed structures resulting in lower porosity. The mechanism requires further investigation; it is possible that more dispersed CB structures exert a greater capillary force on the polymer solution, pinning it within the structure.

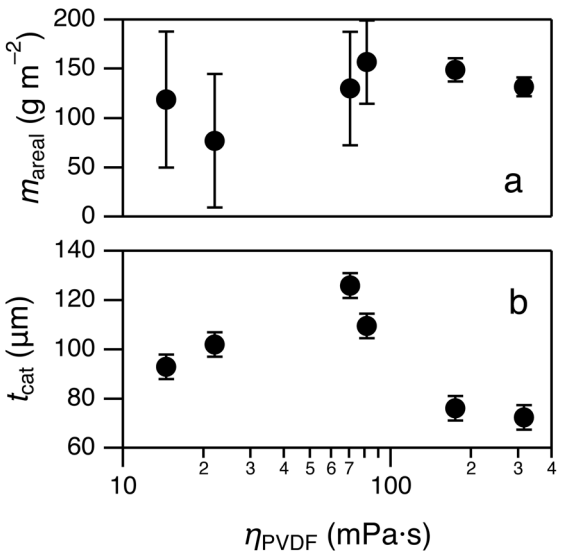

Fig. 8 Properties of formed cathodes of NMC811/CB/PVDF (95 : 5 : 5 w/w/w) across a series of different PVDF/NMP solution viscosities, η_{PVDF}. (a) Areal mass loading, m_{areal}, of the composite cathodes and (b) thicknesses of cathodes produced using a draw down velocity of 5.8 mm s^{-1} and a gap height of 285 μm (see SI Table 8 for full characterisation of these cathodes.).

The dry structure of the cathodes cannot be predicted solely from viscosity nor the viscoelastic loss tangent, but these rheological measurements may serve to outline design rules for slurry testing. For example, samples with a more elastic CB network ($\tan\delta < 0.4$) do not exhibit vertical stratification. Likewise, η_{PVDF} must be greater than 128 mPa s to form a homogeneously dispersed cathode. Comparison with other materials systems will be useful for evaluating the robustness of these design rules.

Cathodes were assembled into half-coin cells and cycled for 100 cycles at a rate of 1C based on a theoretical capacity for NMC811 of 200 mA h g^{-1}. In order to test replicates, the areal mass loading was allowed to vary between 50 and 160 g m^{-2}, as it was difficult to control the thickness of cathodes made using low-viscosity PVDF. The areal loading and thickness of all half-cell cathodes is tabulated in SI Table 8. The first specific discharge curves at 1C are shown in Fig. 9a for each homopolymer binder. The best-performance discharge capacity increases monotonically with the viscosity of the binder solution. The best performing cell (H320) exhibits a first discharge capacity at 1C of 165 mA h g^{-1}, which is at low end of the range for NMC811 at 1C (163–185 mA h g^{-1}), as reported by Savina and Abakumov in an extensive meta-analysis.[48] The specific discharge capacity from the second formation cycle at C/20 is presented in Fig. 9c alongside the first specific discharge capacity at 1C. There is much less variability between replicate cells during the formation cycles, especially for cells formed from a higher viscosity binder solution. The formation data roughly reflects the same trend as the yield stress, with a minimum around $\eta_{PVDF} = 40$ mPa s. There remains a slight trend towards higher performance for samples made from higher viscosity binder solutions.

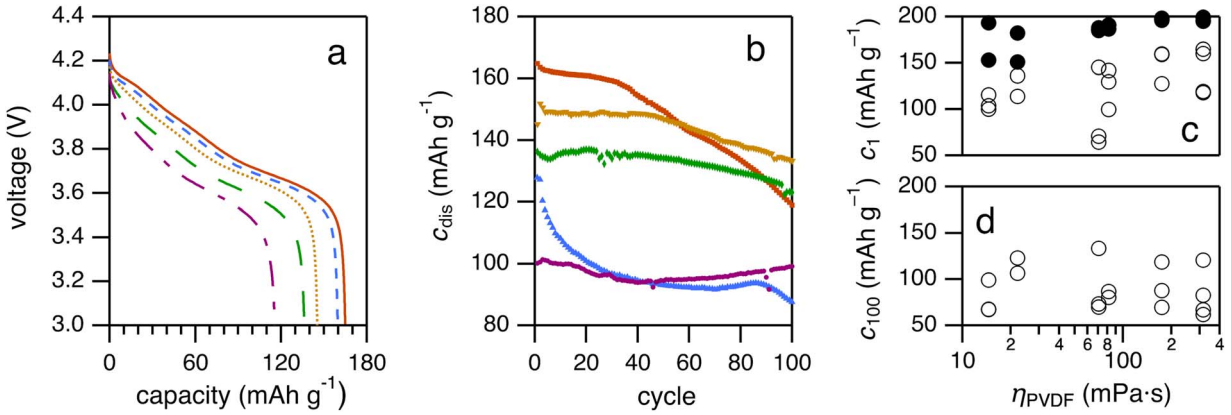

Fig. 9 Battery half-cell testing data for NMC811/CB/PVDF cathodes formed from PVDF solutions of varying viscosity. (a) Discharge curves for the first cycle at 1C for cells comprising H15 (- — -), H20 (— —), H70 (· · ·), H180 (– –) and H320 (——) (b) Capacity fade for selected cells over 100 cycles at 1C comprising H15 (●), H20 (♦), H70 (▼), H180 (▲) and H320 (■). (c) Second formation-cycle discharge (●) at C/20 and first discharge at 1C (○) for all cells. (d) 100th specific discharge capacity, c_{100}, for all half-cells.

Selected capacity fade curves are shown for each sample in Fig. 9b (capacity fade data for all of the cells tested are shown in SI Section 19) and the capacity retention after 100 cycles is shown in Fig. 9d. Under these lab-scale conditions for cathode formation, there is not a significant correlation between cell performance during cycling and the viscosity of the solution from which it was formed. More realistic testing conditions (*e.g.* full cell, pouch cell) and reliable coating and drying processes will be required optimise battery performance with respect to formulation and processing. Discharge curves and dQ/dV curves for both formation and cycling are aviaiable in SI Section 20.

4 Conclusions

This work demonstrates that blending polymer binders is a practical strategy for reliably manipulating the rheological properties of a slurry without reducing the solids loading. The viscosity of cathode slurries can be varied by changing the molecular weight of the homopolymer binder, but batch-wise variations in the chemical properties (*e.g.* crystallinity) lead to less predictable behaviour.

Samples of PVDF vary in their solubility in NMP due to differing levels of crystallinity (an artefact of manufacturing or storage). A small reduction in the soluble fraction of PVDF is enough to drive a dispersed CB gel structure to percolate. In this study, incomplete binder solubility correlated with thixotropy in the slurry and a much broader size distribution of colloidal CB. Very small variations in the PVDF : CB ratio (*e.g.* due to reduced binder solubility) significantly impact the structure and rheological properties of the slurry. Blending fully soluble binders together eliminates flow hysteresis and leads to uniformly dispersed CB gels.

The viscosity of PVDF/NMP solutions is systematically varied from 15 to 320 mPa s and blended with NMC811 and CB to yield slurries with a constant solids loading of 43.1 wt%. The viscosity of the resulting cathode slurry does not increase monotonically with the viscosity of the binder solution, rather, it shows a minimum around binder-solution viscosities of 40 mPa s. Decomposing the contributions to viscosity at a high shear rate, we find that the structure of carbon black dominates, followed by the effects of binder chain entanglements and the presence of 25 vol% NMC has very little contribution to the viscosity of the slurry. As the viscosity of the binder solution increases, the effects of chain entanglements increase relative to the effects of CB structure, leading to a minimum in both the viscosity and yield stress of the slurry. Understanding the interplay of polymer viscosity with carbon black structure is essential for formulating slurries that remain homogeneous whilst drying.

At all viscosities, CB colloidal particles gel, evident in the shear-thinning behaviour of slurries. The CB gel increases the viscosity and elasticity of slurries, resisting the sedimentation of NMC particles during the film drying process. The size of CB agglomerates depends on both the viscosity of the binder solution and the effective ratio of CB : PVDF. More viscous slurries have larger CB particles because more of the mechanical energy supplied is dissipated as heat rather than deagglomerating the CB. Slurries in which the PVDF : CB ratio is decreased transition from a dispersed CB structure to a percolated CB structure that can be identified by thixotropy in a slurry. The PVDF : CB ratio decreases in the presence of NMC, because CB coats the NMC surface. PVDF samples that are not fully soluble also exhibit a reduced PVDF : CB ratio that leads to thixotropy. Controlling the ratio of free CB to dissolved PVDF is critical to the gelled properties of a slurry.

The aggregation behaviour of CB has often been attributed to depletion interactions or bridging flocculation, but we find that neither of these mechanisms is plausible. The concentration of binder is too high to cause a bridging flocculation, and the binder measurably adsorbs onto CB, precluding depletion interactions. Instead, PVDF sterically stabilises CB colloids by adsorbing onto the surface of agglomerates.

Variations in the mass loading of punched cathodes decrease significantly when the viscosity of the binder solution is greater than 128 ± 46 mPa s because the increased cohesive

energy prevents lateral flow along the current collector. Similarly, these films exhibit a more homogeneous distribution of NMC particles and no evidence of vertical segregation nor cracking. The porosity of cathodes can be largely explained by the type of CB gel that forms: percolated CB structures (thixotropic slurries) form more porous electrodes whilst well-dispersed CB gels form denser cathodes.

The first discharge capacity of champion cells increases with the viscosity of the binder solution, but the effect diminishes as the cells are cycled. Viscosity has a significant effect on the structure and flowability of cathode slurries, extending to the mass loading and thickness of dry cathodes. Improved control over the properties of the cathode slurry will allow for more reproducible batches, less wastage and higher energy densities.

Author contributions

Abarasi Hart conceptualization, methodology, validation, investigation, formal analysis, writing – original draft. Xuesong Lu investigation, formal analysis, writing – review & editing. Georgia Englezou investigation. Laura Wheatcroft investigation. Chirag Patel investigation. Joe C. Stallard methodology. Samuel G. Booth investigation, methodology, writing – review & editing. Charles Stothard resources, methodology. Norman A. Fleck methodology, writing – review & editing. Stephen J. Ebbens methodology, resources, writing – review & editing. Beverley J. Inkson methodology. Serena A. Cussen resources, writing – review & editing, supervision, funding acquisition. Denis J. Cumming resources, methodology. Alisyn J. Nedoma conceptualization, formal analysis, investigation, data curation, writing – review & editing, supervision.

Conflicts of interest

There are no conflicts to declare.

Data availability

The data supporting this article have been included as part of the supplementary information (SI) and the relevant SI Sections, Figures and Tables are referenced within the article. Battery specific requirements: Each battery replicate is named with its areal mass loading and thickness in SI Table 7. Discharge capacity data in the main article Fig. 9c and d are reported for each replicate instead of averaging over the cells. C-rates are reported based on the theoretical capacity of NMC811. The mass composition of each sample is given in SI Table 5, and the electrode size and geometry are reported in the main article Section 2.3. Formation cycling data is shown in main article Fig. 9c. SI Section 18 presents the voltage charging and discharging curves and dQ/dV curves for both formation cycles and selected cycles for each cell replicate along with the capacity fade and coulombic efficiency across 100 cycles at 1C. Supplementary information is available. See DOI: https://doi.org/10.1039/d5ta07131c.

Acknowledgements

This work was supported by the Faraday Institution grant number FIRG017. DJC and XL acknowledge the Faraday Institution grant number FIRG015. AJN gratefully acknowledges helpful discussions with Siddharth V. Patwardhan, Jon Howse, Emma Kendrick, Alan Dunbar, Chris Holland, Richard Hodgkinson and Andrew Campbell.

Notes and references

1 High-energy battery technologies, *The Faraday Institution Technical Report*, 2020.
2 J.-M. Tarascon and M. Armand, *Nature*, 2001, **414**, 359–367.
3 S. G. Booth, A. J. Nedoma, N. N. Anthonisamy, P. J. Baker, R. Boston, H. Bronstein, S. J. Clarke, E. J. Cussen, V. Daramalla, M. De Volder, S. E. Dutton, V. Falkowski, N. A. Fleck, H. S. Geddes, N. Gollapally, A. L. Goodwin, J. M. Griffin, A. R. Haworth, M. A. Hayward, S. Hull, B. J. Inkson, B. J. Johnston, Z. Lu, J. L. MacManus-Driscoll, X. Martínez De Irujo Labalde, I. McClelland, K. McCombie, B. Murdock, D. Nayak, S. Park, G. E. Pérez, C. J. Pickard, L. F. J. Piper, H. Y. Playford, S. Price, D. O. Scanlon, J. C. Stallard, N. Tapia-Ruiz, A. R. West, L. Wheatcroft, M. Wilson, L. Zhang, X. Zhi, B. Zhu and S. A. Cussen, *APL Mater.*, 2021, **9**, 109201.
4 T. Entwistle, E. Sanchez-Perez, G. J. Murray, N. Anthonisamy and S. A. Cussen, *Energy Rep.*, 2022, **8**, 67–73.
5 M. Keppeler, S. Roessler and W. Braunwarth, *Energy Technol.*, 2020, **8**, 2000183.
6 Z. Lu, B. Zhu, B. W. B. Shires, D. O. Scanlon and C. J. Pickard, *J. Chem. Phys.*, 2021, **154**, 174111.
7 P. S. Grant, D. Greenwood, K. Pardikar, R. Smith, T. Entwistle, L. A. Middlemiss, G. Murray, S. A. Cussen, M. J. Lain, M. J. Capener, M. Copley, C. D. Reynolds, S. D. Hare, M. J. H. Simmons, E. Kendrick, S. P. Zankowski, S. Wheeler, P. Zhu, P. R. Slater, Y. S. Zhang, A. R. T. Morrison, W. Dawson, J. Li, P. R. Shearing, D. J. L. Brett, G. Matthews, R. Ge, R. Drummond, E. C. Tredenick, C. Cheng, S. R. Duncan, A. M. Boyce, M. Faraji-Niri, J. Marco, L. A. Roman-Ramirez, C. Harper, P. Blackmore, T. Shelley, A. Mohsseni and D. J. Cumming, *J. Phys.: Energy*, 2022, **4**, 042006.
8 W. Bauer and D. Nötzel, *Ceram. Int.*, 2014, **40**, 4591–4598.
9 A. Kraytsberg and Y. Ein-Eli, *Adv. Energy Mater.*, 2016, **6**, 1600655.
10 D. Gastol, M. Capener, C. Reynolds, C. Constable and E. Kendrick, *Mater. Des.*, 2021, **205**, 109720.
11 C. D. Reynolds, P. R. Slater, S. D. Hare, M. J. Simmons and E. Kendrick, *Mater. Des.*, 2021, **209**, 109971.
12 J. P. Sullivan and A. Bose, *Electrochem. Commun.*, 2022, **141**, 107353.
13 W. B. Hawley and J. Li, *J. Energy Storage*, 2019, **26**, 100994.
14 C. D. Reynolds, S. D. Hare, P. R. Slater, M. J. H. Simmons and E. Kendrick, *Energy Technol.*, 2022, **10**, 2200545.
15 M. Wang, D. Dang, A. Meyer, R. Arsenault and Y.-T. Cheng, *J. Electrochem. Soc.*, 2020, **167**, 100518.

16 D. L. Wood, J. D. Quass, J. Li, S. Ahmed, D. Ventola and C. Daniel, *Drying Technol.*, 2018, **36**, 234–244.
17 G. Lutringer, B. Meurer and G. Weill, *Polymer*, 1991, **32**, 884–891.
18 M. Okabe, R. Wada, M. Tazaki and T. Homma, *Polym. J.*, 2003, **35**, 798–803.
19 R. Jung, M. Metzger, F. Maglia, C. Stinner and H. A. Gasteiger, *J. Electrochem. Soc.*, 2017, **164**(7), A1361–A1377.
20 H.-J. Noh, S. Youn, C. S. Yoon and Y.-K. Sun, *J. Power Sources*, 2013, **233**, 121–130.
21 J. K. Morzy, W. M. Dose, P. E. Vullum, M. C. Lai and A. Mahadevegowda, *ACS Appl. Energy Mater.*, 2024, **7**, 3945–3956.
22 L. Wheatcroft, A. Bird, J. C. Stallard, R. L. Mitchell, S. G. Booth, A. J. Nedoma, M. F. L. De Volder, S. A. Cussen, N. A. Fleck and B. J. Inkson, Fracture Testing of Lithium-Ion Battery Cathode Secondary Particles in-situ inside the Scanning Electron Microscope, in *Batteries Supercaps*, 2023, vol. 7, p. e202300032.
23 B. Zhu, Y. Ning, Z. Xu, G. Wei and J. Qu, *J. Mater. Chem. A*, 2024, **12**, 1671–1684.
24 M. E. Spahr, D. Goers, A. Leone, S. Stallone and E. Grivei, *J. Power Sources*, 2011, **196**, 3404–3413.
25 Y. Aoki, A. Hatano and H. Watanabe, *Rheol. Acta*, 2003, **42**, 209–216.
26 J. J. Richards, P. Z. Ramos and Q. Liu, *Front. Phys*, 2023, **11**, 1245847.
27 S. H. Sung, S. Kim, J. H. Park, J. D. Park and K. H. Ahn, *Materials*, 2020, **13**, 4544.
28 P. De Gennes, *J. Phys.*, 1976, **37**, 1445–1452.
29 Á. González García, M. M. Nagelkerke, R. Tuinier and M. Vis, *Adv. Colloid Interface Sci.*, 2020, **275**, 102077.
30 V. Wenzel, H. Nirschl and D. Nötzel, *Energy Technol.*, 2015, **3**, 692–698.
31 G. Legrand, S. Manneville, G. H. McKinley and T. Divoux, *Macromolecules*, 2023, **56**, 2298–2308.
32 C.-C. Chang, L.-J. Her, H.-K. Su, S.-H. Hsu and Y. T. Yen, *J. Electrochem. Soc.*, 2011, **158**, A481.
33 J. Entwistle, R. Ge, K. Pardikar, R. Smith and D. Cumming, *Renewable Sustainable Energy Rev.*, 2022, **166**, 112624.
34 M. Weber, J. K. Mayer and A. Kwade, *Energy Technol.*, 2023, **11**, 2201299.
35 W. Bauer, D. Nötzel, V. Wenzel and H. Nirschl, *J. Power Sources*, 2015, **288**, 359–367.
36 K. M. Kim, W. S. Jeon, I. J. Chung and S. H. Chang, *J. Power Sources*, 1999, **83**, 108–113.
37 G.-W. Lee, J. H. Ryu, W. Han, K. H. Ahn and S. M. Oh, *J. Power Sources*, 2010, **195**, 6049–6054.
38 S. P. Rwei, I. Manas-Zloczower and D. L. Feke, *Polym. Eng. Sci.*, 1990, **30**, 701–706.
39 Y. I. Kwon, J. D. Kim and Y. S. Song, *J. Electron. Mater.*, 2015, **44**, 475–481.
40 D. Grießl, K. Huber, R. Scherbauer and A. Kwade, *Adv. Powder Technol.*, 2021, **32**, 2280–2288.
41 J. B. Hipp, J. J. Richards and N. J. Wagner, *J. Rheol.*, 2019, **63**, 423–436.
42 F. Ma, Y. Fu, V. Battaglia and R. Prasher, *J. Power Sources*, 2019, **438**, 226994.
43 H. A. Barnes, *J. Non-Newtonian Fluid Mech.*, 1999, **81**, 133–178.
44 Targray, NMC811 Powder Specifications, https://www.targray.com/li-ion-battery/cathode-materials/nmc.
45 S. L. Morelly, R. M. Saraka, N. J. Alvarez and M. Tang, *Batteries*, 2024, **10**, 46.
46 V. Trappe and P. Sandkühler, *Curr. Opin. Colloid Interface Sci.*, 2004, **8**, 494–500.
47 S. Nurkhamidah and E. M. Woo, *J. Appl. Polym. Sci.*, 2011, **122**, 1976–1985.
48 A. A. Savina and A. M. Abakumov, *Heliyon*, 2023, **9**, e21881.